Available online at www.sciencedirect.com
SCIENCE DIRECT®
International Journal of Heat and Mass Transfer 47 (2004) 1423–1432
International Journal of HEAT and MASS TRANSFER
www.elsevier.com/locate/ijhmt

Solidification of a binary mixture in a shear flow

S. Mergui *, B. Feroual, D. Gobin, C. Bénard

FAST, UMR CNRS 7608 (Universities Paris VI and Paris XI, CNRS), Campus Universitaire, Bâtiment 502, 91405 Orsay cedex, France

Received 15 January 2003

Abstract

This paper presents experimental results concerning the solidification of a binary aqueous solution flowing along a cold surface. Forced convection in the liquid phase is assumed to dominate over possible natural convection effects at the interface and the influence of the initial solute concentration is analyzed. Solute rejection at the interface is shown to influence the equilibrium temperature at the solidification front and the time evolution of the solid phase. Comparison with the numerical solution of a simple thermal phase change model shows that the solidification dynamics is compatible with a porous structure of the solid phase (solid fraction about 0.90), accounting for dendritic structure at the microscale.

1. Introduction

Solidification of binary alloys has been the subject of many studies in recent years. The presence of natural convection due to the phase change process itself is known to have a strong influence on the dynamics of the process, as reported by Davis et al. [1] or experimentally studied by Prescott and Incropera [2] or Tanny [3]. Due to the combined temperature and composition gradients, solidification along a flat plate is affected by double diffusive instabilities (horizontal plate) or thermosolutal convection (vertical plate), both in terms of solidification rate and of mush structure. Many experiments, models and stability studies have been dedicated to this problem in the heat transfer literature in order to characterize the complex interaction between the flow structure and the dynamics of the interfacial growth region. Otherwise, many studies have dealt with features of water–ice interface in external or internal forced flow during freezing or melting processes, as referred by Epstein and Cheung [4], but very few studies are concerned with binary substances. The existing studies deal with the effect of an imposed shear flow on the stability of directional solidification of binary alloys and are investigated by theoretical or numerical approach (Forth and Wheeler [5,6], Chung and Chen [7] and very recently Tangthieng and Cheung [8]).

The purpose of the present work is to partially uncouple the heat and mass transfer mechanisms at a solidifying interface, by limiting the effects of natural convection on the phase change process. In opposition to the usual practice where natural convection is inhibited to impose a purely diffusive heat and species transfer, the present approach aims at imposing a forced flow at the solid–liquid interface. Thus, the influence of a convective flow at the interface is retained, but there is no (or little) feedback of the interface structure and dynamics on the flow itself. More precisely, the scope of this paper is to experimentally tackle the problem of solidification of a binary mixture along a horizontal flat plate in a forced laminar flow. Under moderate Reynolds number laminar shear flow conditions, the heat and species transfer at the growing interface is dominated by the forced flow, although gravity effects may be detected when considering growth either from the top or from the bottom surface of the plate.

Accurate local temperature measurements of the top interface have been performed. Local thermodynamic equilibrium being assumed, those temperature measurements provide experimental values for the local front concentration and point out the importance of

* Corresponding author. Tel.: +33-1-69-15-80-73; fax: +33-1-69-15-80-60.
E-mail address: mergui@fast.u-psud.fr (S. Mergui).

0017-9310/$ - see front matter © 2003 Elsevier Ltd. All rights reserved.
doi:10.1016/j.ijheatmasstransfer.2003.10.003

Nomenclature

C_0	initial concentration of the solution (%wt.)
$h(t)$	instantaneous heat transfer coefficient (W/m^2 °C)
$h_{\lim}$	heat transfer coefficient at the end of the experiment (W/m^2 °C)
k_L	thermal conductivity of the liquid phase (W/m °C)
k_S	thermal conductivity of the solid phase (W/m °C)
L	length of the exchanger (m)
L_F	latent heat of fusion (J/kg)
$q_L(t)$	heat flux at the solid–liquid interface (W/m^2)
$s(t)$	instantaneous front position (m)
$s_{\max}$	maximal solid thickness (m)
Ste	Stefan number $= c_{PS}\,\Delta T_S/L_F$
t	time (s)
T_L	initial temperature of the liquid phase (°C)
$T_F(t)$	instantaneous front temperature (°C)
$T_{Liq}(C_0)$	equilibrium interfacial temperature for a solution at concentration C_0 (°C)
T_P	wall exchanger temperature (°C)
T_S	solid phase temperature (°C)
V	velocity of the liquid phase in the experimental cell (m/s)
x	distance from the leading edge of the exchanger (m)
z	vertical distance from the exchanger (m)
ΔT_L	Temperature difference between the liquid phase and the liquidus curve $= T_L - T_{Liq}(C_0)$ (°C)
ΔT_S	Temperature difference between the exchanger and the liquidus curve $= T_{Liq}(C_0) - T_P$ (°C)

Greek symbols

α_S	Thermal diffusivity of the solid phase (m^2/s)
Φ	Volumic solid fraction
ρ_S	Density of the solid phase (kg/m^3)

solute redistribution at the interface during the solidification process. Thus, depending on the solidification parameters, the time evolution of solute rejection is known and its consequence on the local dynamics of the interface is directly observed on the shape of the front profile.

The experimental results, in terms of the time evolution of the interface position, are compared to a simple thermal model, and the influence of solute rejection at the interface is exhibited through the displacement of the interface temperature at the solidifying front.

2. Presentation of the experiments

2.1. Experimental setup

The experimental cell, presented in Fig. 1a, consists of a horizontal cold heat exchanger (width = 0.04 m, length = L = 0.20 m, height = 0.02 m) located in the midplane of a channel (height = 0.25 m, width = 0.20 m, length = 0.70 m) where a binary solution of NH_4Cl at uniform concentration is circulated. A set of honeycombed structures are placed at the entrance of the channel to ensure laminar flow and uniform velocity all along the experimental cell. Particles have been introduced in the solution and preliminary visualizations have been performed to characterize the flow structure and the velocity magnitude around the exchanger. The temperature of the mixture flow is controlled and maintained constant at T_L using two vertical heat exchangers located upstream of the experimental cell (Fig. 1b).

The lateral walls of the channel cavity are made of transparent sheets allowing for visualizing the front growth. At the initial time, the horizontal exchanger temperature is decreased below the temperature given by the liquidus curve of the phase diagram of the solution, and solidification starts at the top and bottom surfaces of the exchanger. Visualizations are carried out using a thin vertical laser sheet parallel to the mean flow, located in the mid-width of the cold exchanger, allowing for measurements of the time evolution of the vertical front position. Measurements are performed at two locations from the leading edge of the exchanger: $x_1 = 55.2$ mm and $x_2 = 86.5$ mm (Fig. 2a).

The temperature of the cold plate is carefully monitored using thermocouples embedded at the inlet and outlet of the exchanger and the mean final stationary value is used to define the governing parameters. A rack of K-type calibrated thermocouples, located at $x_3 = 150$ mm from the leading edge, give the time evolution of the temperature distribution in the liquid and the solid phases in the growth direction, with an absolute precision of 0.1 K. Coupled to local observations of the solidification front position, those temperature measurements allow for the determination of instantaneous values of the local front temperature.

To visualize the effect of the solute rejection on the liquid phase, a shadowgraph technique is used to detect the spatial variations of the density gradient. A parallel light beam is generated using a white light source located

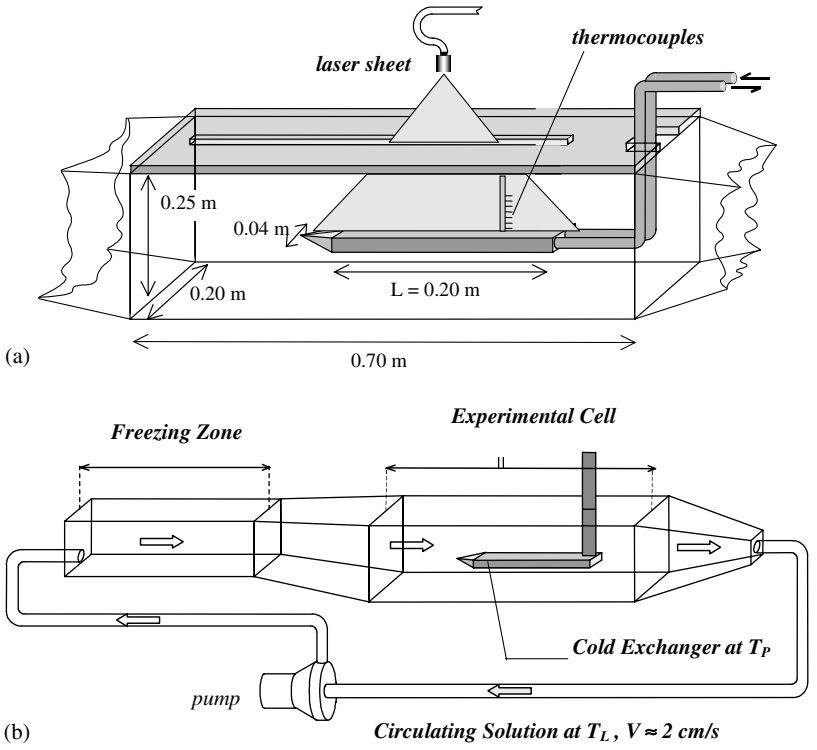

Fig. 1. Experimental setup: (a) experimental cell; (b) thermal regulated circulation loop.

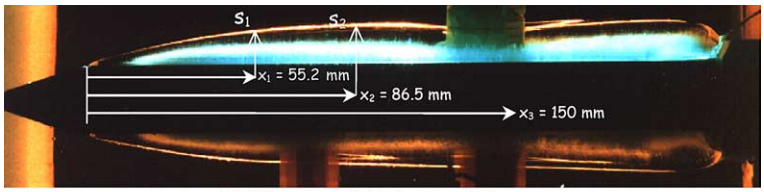

(a) Experiment # 1 (pure water)

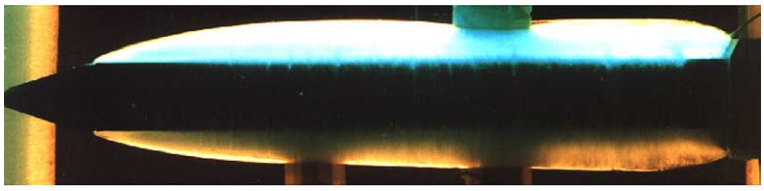

(b) Experiment #2 (C_0 = 4 %)

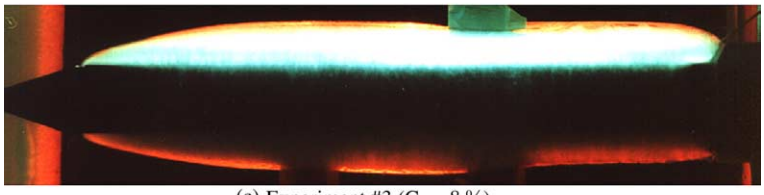

(c) Experiment #3 (C_0 = 8 %)

Fig. 2. Visualization of the solid phase at $t \approx 7$ h, for the three experiments.

Table 1
Parameters of the experiments

	Exp. #1 $C_0 = 0\%$	Exp. #2 $C_0 = 4\%$	Exp. #3 $C_0 = 8\%$
$T_{Liq}(C_0)$ (°C)	0	−2.55	−5.46
T_P (°C)	−8.5	−11.4	−14.5
T_L (°C)	6.7	3.7	0.5
ΔT_S (°C) $= T_{Liq}(C_0) - T_P$	8.5	8.85	9.05
ΔT_L (°C) $= T_L - T_{Liq}(C_0)$	6.7	6.21	5.95
Ste	0.052	0.054	0.055
$\Delta T_S/\Delta T_L$	1.27	1.43	1.52

on the back of the experimental cell in the focal plane of a lens. Images are taken through a translucent screen placed along the front wall of the experimental cell.

2.2. Set of experiments

The thermal conditions imposed to this system are the Stefan number based on the temperature difference ΔT_S between the liquidus curve and the exchanger and the superheating parameter, the temperature difference ΔT_L between the fluid and the liquidus curve. In this study, the fluid velocity is kept constant ($V \approx 0.02$ m/s giving rise to a Reynolds number calculated with the length of the exchanger of about 2500) and three different experiments have been performed to study the influence of the initial solute concentration in the liquid phase on the dynamics of solidification and on the interface characteristics. Experiments have been repeated to verify the reproducibility of the observations and measurements. The reference experiment is obtained with pure water (concentration 0 %wt.), because it refers to a classical Stefan problem where only thermal interface conditions are involved. The other experiments are performed using 4 and 8 %wt. NH_4Cl aqueous solution, characterized by a segregation coefficient equal to zero (in theory, the concentration in the solid phase is zero). The objective of this study is to keep the similarity of the governing parameters. Since the corresponding liquidus equilibrium temperatures are 0, −2.55 and −5.46 °C respectively, the operating conditions are such that the Stefan number (the driving temperature difference ΔT_S) and the resisting force (the liquid temperature difference ΔT_L) are kept nearly constant (see Table 1).

3. Model

The analysis of the experimental results is based on a comparison with numerical simulations performed with a 1D finite volume code solving the conduction phase change problem. The original version of the code was dedicated to the Stefan problem including heat diffusion in both phases and energy balance at the solid–liquid interface. The classical Landau transformation technique is used in the solid phase and the interface velocity is iteratively determined at each time step to satisfy the energy balance at the moving front. The code has been validated against the classical Neumann solution [9].

For the present study, the code has been adapted to account for a convective flux condition at the interface on the liquid side and to allow for time variations of the interface and cold plate temperatures. As we do not solve the heat and fluid flow problem in the liquid channel, the flux condition at the S–L interface on the liquid side is accounted for by the following expression:

$$q_L(t) = h(t)(T_F(t) - T_L), \tag{1}$$

where $h(t)$ is the heat transfer coefficient at a given x position along the exchanger.

The local heat balance at the interface writes, at time t:

$$k_S\left(\frac{\partial T_S}{\partial z}\right)_{\text{interface}} - h(t)(T_L - T_F(t)) = \rho_S L_F \frac{ds(t)}{dt}. \tag{2}$$

A quasi-steady state of the phenomena under study is assumed. This approximation is validated from the comparison between the characteristic time of the exchanger temperature variation, τ, and the characteristic time of heat diffusion in the solid phase, $\tau_d = s^2(\tau)/\alpha_S$, where $s(\tau)$ is the solid thickness at τ. In our experiments $\tau \approx 1800$ s and $s(\tau) \approx 14$ mm (see Section 4.4), then $\tau \gg \tau_d$ ($\tau \approx 11\tau_d$ using $\alpha_S \approx 1.2 \times 10^{-6}$ (pure ice)). Except at the very beginning of the experiment, the quasi-stationary regime is valid providing linear temperature profiles in the solid phase (see Section 4.3). Under this assumption, we can write Eq. (2) as

$$k_S\frac{T_F(t) - T_P(t)}{s(t)} - h(t)(T_L - T_F(t)) = \rho_S L_F \frac{ds(t)}{dt}. \tag{3}$$

In this equation, $h(t)$ has to be estimated and since we are interested in the analysis of a possible variation of the interface conditions during the solidification process, the actual interface temperature T_F is not known a priori.

4. Experimental results

4.1. Visualizations

Visualization of the solid phase for the three experiments is illustrated in Fig. 2, 7 h after the beginning of the experiment. The global shape of the solid is similar in the three cases: due to dynamic effects, the solid thickness is smaller near the leading edge than in the middle of the exchanger. We can observe a difference in the structure of the solid phase, between experiment #1 (pure water) and experiments #2 and #3. For pure water, the white region near the exchanger is the consequence of air bubbles trapped at the beginning of the experiment, when the kinetic of solidification is high. The solid becomes transparent when solidification slows down. For salt solution, no bubbles emission has been observed and all the solid phase remains white and opaque all along the experiment. This aspect is due to the solute rejected during solidification, which is trapped in the solid when the kinetic is high. Indeed, visualizations carried out a very long time after the beginning of the experiment (typically four days after) showed salt aggregates in a perfectly transparent solid.

The solute rejected during solidification is denser than the initial solution and falls down due to gravity effects. Concerning the upper part of the experiment, the rejected solute is trapped in the growing solid or is swept along by the forced flow. A very thin solutal layer is then generated in the vicinity of the upper interface and density variations cannot be detected using shadowgraphy. On the contrary, gravity effects provide a large solutal layer near the lower front and shadow regions can be easily visualized. A set of images obtained by shadowgraphy (Fig. 3) illustrates the time evolution of the density variation region during experiment #3.

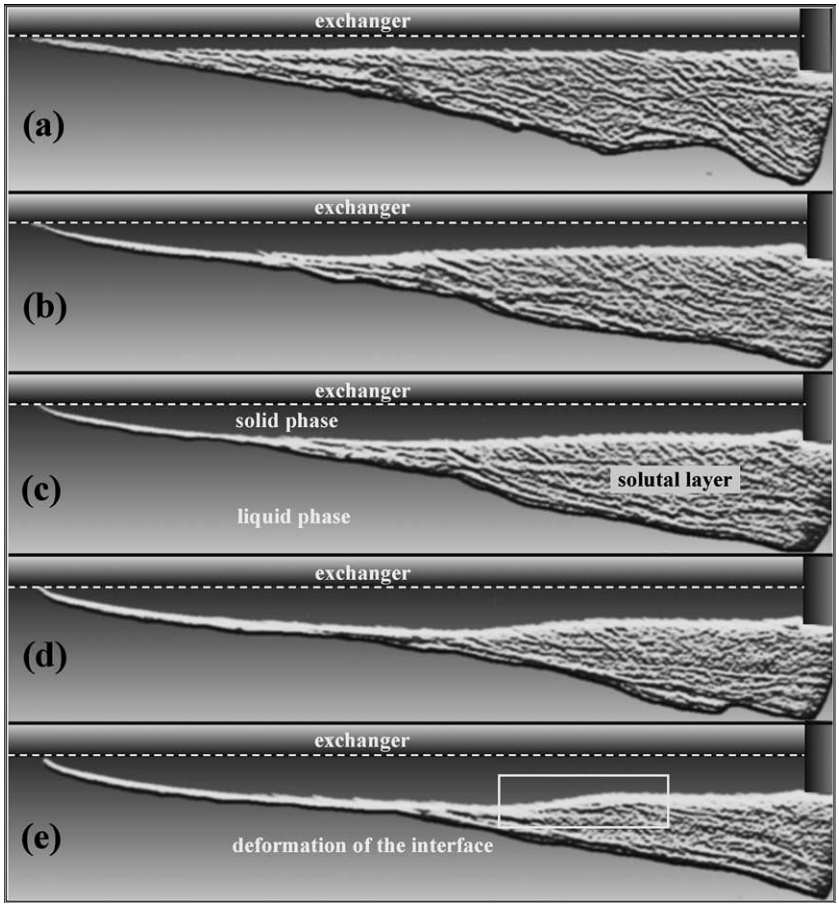

Fig. 3. Visualization of the time evolution of the solute rejection at the lower front for experiment #3. (a) $t = 14$ min, (b) $t = 1$ h 13 min, (c) $t = 1$ h 58 min, (d) $t = 2$ h 54 min and (e) $t = 4$ h 01 min. The cold exchanger surface is represented by the white dotted line, the solid phase corresponds to the gray region just below and the solid/liquid interface to the white line.

Similar features have been observed for experiment #2. The resulting pattern is the combination of gravity and solute diffusion effects giving rise to vertical solute transport and the forced flow effect creating horizontal solute transport. At the beginning of the experiment, the solidification kinetic is high and a density variation region is observed all along the exchanger (Fig. 3a). During the experiment, the solutal layer is carried along by the forced flow and goes away from the leading edge of the exchanger as the solidification rate decreases. Related to that observation, we can detect a deformation of the solid shape resulting from a slowing down of the interface progression due to the accumulation of the solute in the density variation region, as indicated in Fig. 3e.

If we focalize our attention on the structure of the lower solid, it can be seen a wavy shape of the interface due to thermal natural convective motions that develop in the liquid phase. Consequently, mixed convection governs the transfers at the lower interface. The problem becomes complex and is not quantitatively tackled in this study. The results presented in the following sections concern the upper region only.

4.2. Heat transfer coefficient

The heat transfer coefficient is evaluated from the experimental results related to experiment #1. Indeed, for pure water, the interface temperature is $T_F(t) = 0\ ^\circ\mathrm{C}$ $\forall t$. Knowing the experimental time history of $s(t)$ and $v(t) = \mathrm{d}s/\mathrm{d}t$, the resolution of Eq. (3) at each time yields the time evolution of the heat transfer coefficient $h_1(t)$ at x_1 and $h_2(t)$ at x_2:

$$h(t) = \frac{k_S}{s(t)} \frac{0\ ^\circ\mathrm{C} - T_P(t)}{T_L - 0\ ^\circ\mathrm{C}} - \rho_S L_F \frac{v(t)}{T_L - 0\ ^\circ\mathrm{C}}. \quad (4)$$

At the beginning of the process, the accuracy on $h(t)$ is about 30% due to the lack of precision in the front velocity measurement when the solidification rate is high. But at this time, the solid thickness is very thin and the temperature gradient in the solid phase is very high. The heat flux coming from the heat exchanger, $k_S(\frac{\partial T_S}{\partial z})_{\mathrm{interface}}$, is then dominating the heat balance equation at the interface and a rough estimation of h is sufficient to analyze the solidification kinetics. At the end of the experiment ($t = t_{\mathrm{final}}$), the front velocity is zero (see next section) and the final heat transfer coefficient is calculated by the following expression:

$$h_{\mathrm{lim}} = \frac{k_S}{s(t_{\mathrm{final}})} \frac{\Delta T_S}{\Delta T_L} \quad (5)$$

with a precision of 6%.

As expected from the visualizations, the final heat transfer coefficient is larger at x_1, where $h_{\mathrm{lim1}} = 240$ W/m^2 °C, than at x_2, where $h_{\mathrm{lim2}} = 209$ W/m^2 °C.

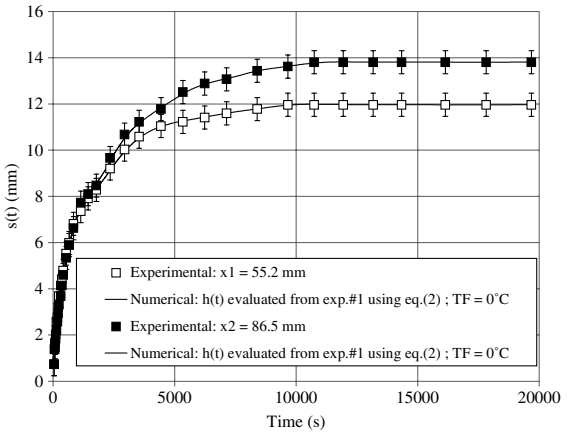

Fig. 4. Experimental and numerical time evolution of the front position for experiment #1 (pure water).

By introducing the experimental tabulated values of $h_1(t)$ at x_1 and $h_2(t)$ at x_2 in the numerical model, we obtain a numerical solution of the interface position at x_1 and x_2, which is compared to the experimental one in Fig. 4. A very good agreement is observed between the results, validating the relevance of the heat transfer coefficient estimation from the experiments and the quasi-stationary model.

The main assumption in the analysis of the results presented below is to consider that the time evolution of the heat transfer coefficient is the same in the three experiments.

4.3. Temperature

Time evolution of the vertical temperature profile in the direction of solidification is reported in Fig. 5 for experiment #2. It can be seen that the temperature distribution in the solid phase is linear, validating the quasi-stationary assumption previously used. Similar feature is observed for the other experiments.

Fig. 6 displays time evolutions of the temperature given by the thermocouples located on the rack initially in the liquid phase, for experiment #2.

The interface temperature measurements performed during experiments #2 and #3 are listed in Table 2 and are illustrated in Fig. 6 for experiment #2. The results show that, for both cases, the interface temperature is approximately the theoretical equilibrium temperature for the corresponding solute concentration, $T_{\mathrm{Liq}}(C_0)$, when the quasi-steady evolution of the process is reached. In the early stage where the front velocity is larger, the interface temperature may be lower than the equilibrium temperature by as much as 1 °C for experiment #2 and 2 °C for experiment #3, due to the effect of the solute redistribution on the phase change temperature.

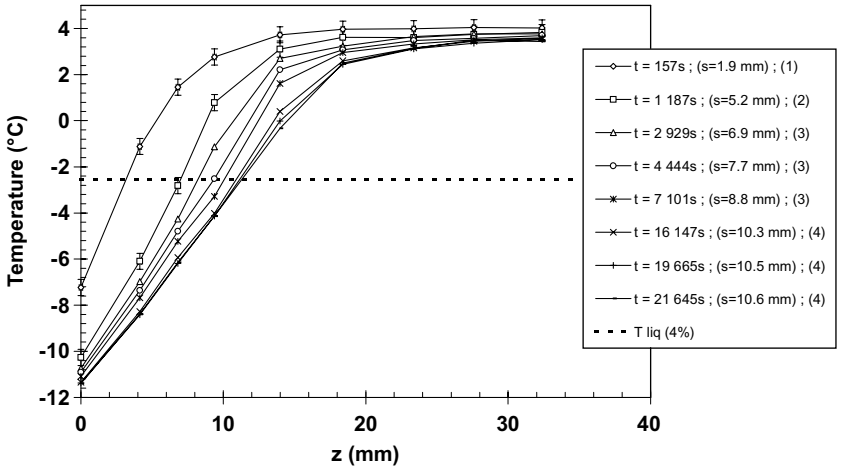

Fig. 5. Time evolution of temperature profiles in the direction of solidification (experiment #2). For each time, the corresponding thickness of the solid phase, s, is indicated between parenthesis as well as the number of thermocouples in the solid phase at this time.

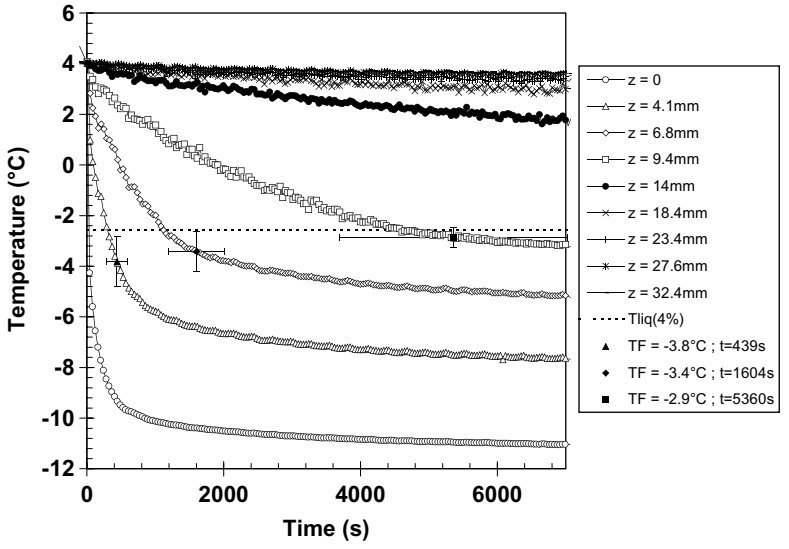

Fig. 6. Time evolution of the signal delivered by nine thermocouples located at different distances from the exchanger for experiment #2 ($x_3 = 150$ mm).

Table 2
Experimental values of the front temperature

	Time (s)	Experimental $T_F(t) = T_{Fexp}(t)$ (°C)
Experiment #2 ($C_0 = 4\%$)	440	-3.8 ± 1.0
$T_{Liq}(C_0) = -2.55$ °C	1604	-3.4 ± 0.8
	5360	-2.9 ± 0.4
Experiment #3 ($C_0 = 8\%$)	668	-7.5 ± 1.6
$T_{Liq}(C_0) = -5.46$ °C	2533	-6.3 ± 1.0
	6224	-5.6 ± 0.8

4.4. Interface position

The experiment is stopped at $t = t_{final}$ when a steady state is reached, characterized by $ds/dt = 0$ and, as previously seen, $T_F(t) = T_{Liq}(C_0)$. From Eq. (3), a theoretical final value of the ice layer thickness can be determined as:

$$s_{max}(C_0) = \frac{k_S}{h_{lim}} \frac{T_{Liq}(C_0) - T_P}{T_L - T_{Liq}(C_0)} = \frac{k_S}{h_{lim}} \frac{\Delta T_S}{\Delta T_L}. \quad (6)$$

Since it is experimentally difficult to impose the same values of ΔT_S and ΔT_L, a slight dispersion may be noticed in the values listed in Table 1. Thus, s_{max} is not strictly identical for the three experiments. Then, to compare the results obtained for different experiments, the experimental time evolution of the interface position will be displayed in terms of $s(t)/s_{max}$.

In Fig. 7, time evolutions of the front position at x_1 and x_2 for both experiments #1 (pure water) and #3 ($C_0 = 8$ %wt.) are represented. Experiment #2 ($C_0 = 4$ %wt.) behaves like experiment #3. Measurements precision is of the same order of magnitude for both locations x_1 and x_2. To lighten the figure, error bars are then represented for the x_1 location only.

The first significant result is that, for a given location, $s(t)/s_{max}$ decreases when C_0 increases. This feature points out the strong effect of the solute redistribution on the solid growth.

In that representation, the front behavior is identical at both locations x_1 and x_2 for the pure water experiment. On the other hand for the 8% experiment, the curve corresponding to x_1 is above the curve related to x_2. In addition, we note that the curve at x_2 does not reach the s_{max} value at $t = t_{final}$, in spite of the fact that the stationary regime has been reached and that the front temperature is the equilibrium temperature. Same feature has been observed for experiment #2.

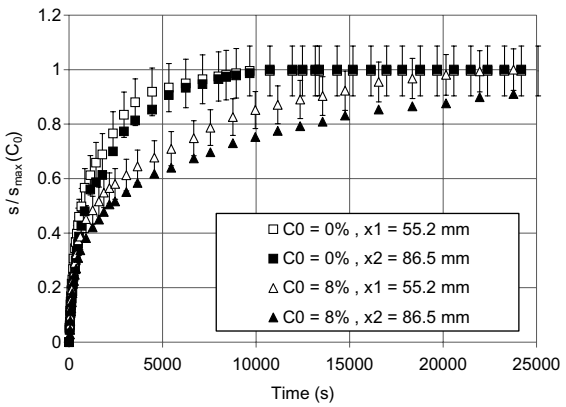

Fig. 7. Time evolution of the experimental front position at x_1 and x_2 for experiments #1 and #3.

If our assumption that the estimation of $h(t)$ is reasonably correct for experiments #2 and #3, this overestimation of s_{max} may arise from an overestimation of k_S, the thermal conductivity of the solid phase (see Eq. (6)). Assuming that the formation of dendrites in the solidification process may result in a solid phase whose volumic solid fraction Φ is not strictly 1, one can suggest the hypothesis that the conductivity of such a "porous" solid is a simple weighted average of the conductivities of the solid and the liquid phases:

$$K_{av} = \Phi k_S + (1 - \Phi) k_L. \quad (7)$$

So, revisiting Eq. (3), one can estimate the corresponding value of Φ in the final stage of the experiment by

$$\Phi = \frac{s(t_{final})/s_{max} - k_L/k_S}{1 - k_L/k_S}. \quad (8)$$

This calculation gives $\Phi \approx 0.90$ for both experiments #2 and #3.

Let us use the time evolution of the heat transfer coefficient estimated from the experimental results and

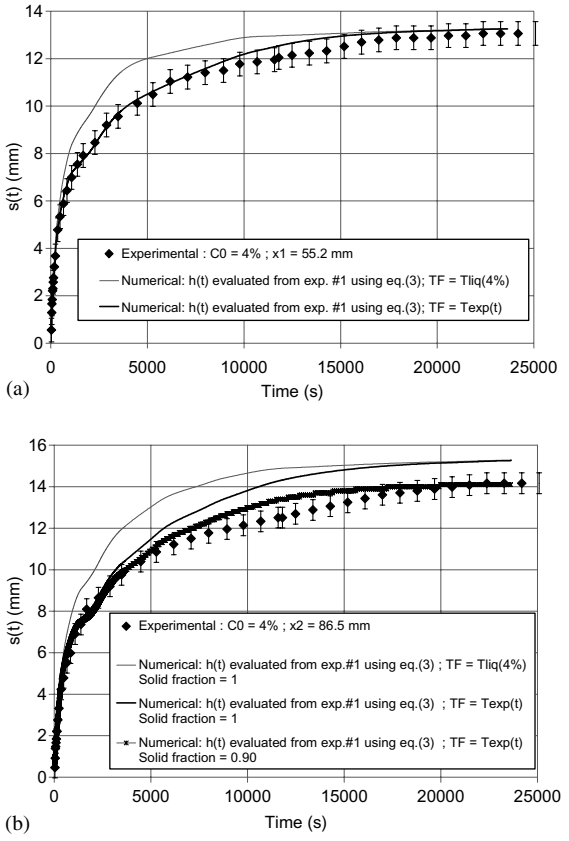

Fig. 8. Experiment #2: comparison between experimental and numerical time evolution of the front position at x_1 and x_2: (a) $x_1 = 55.2$ mm; (b) $x_2 = 86.5$ mm.

the temperature measurements at the interface as the inputs of the numerical code. Figs. 8a (exp. #2) and 9a (exp. #3) displayed the time history of the front position given by the simulation at x_1, compared to the experimental results. It appears very clearly that the solution obtained with a constant interface temperature corresponding to $T_{\mathrm{Liq}}(C_0)$ does not follow the experimental observations, especially in the initial stage of the solidification process. This discrepancy and the good agreement of the variable interface temperature solution with the experiments show that solute rejection at the interface has a noticeable influence on the thermal conditions at the phase change interface and that forced convection is not sufficient to wipe out its effects on the solidification dynamics.

The agreement is not so clear at the x_2 location, where the experimental front positions are significantly below the simulated curves for both the #2 and the #3 experiments (Figs. 8b and 9b). Let us assume that the discrepancies are the effect of the dendritic aspect of the solid phase ($\Phi < 1$). Indeed, when the solid fraction decreases, the relative contribution of the heat flux from the liquid in the heat transfer balance increases and a slowing down of the front progression is expected. The simulations performed with the previous estimation of Φ ($\Phi = 0.90$) are displayed in Figs. 8b and 9b. The corresponding curves are almost entirely within the uncertainty range, except in the central part of the experiment, which might mean that the solid fraction is not constant all along the solidification process, that is, is lower in the initial stage of the process where the kinetic is larger than in the final stage where the quasi-stationary state is reached.

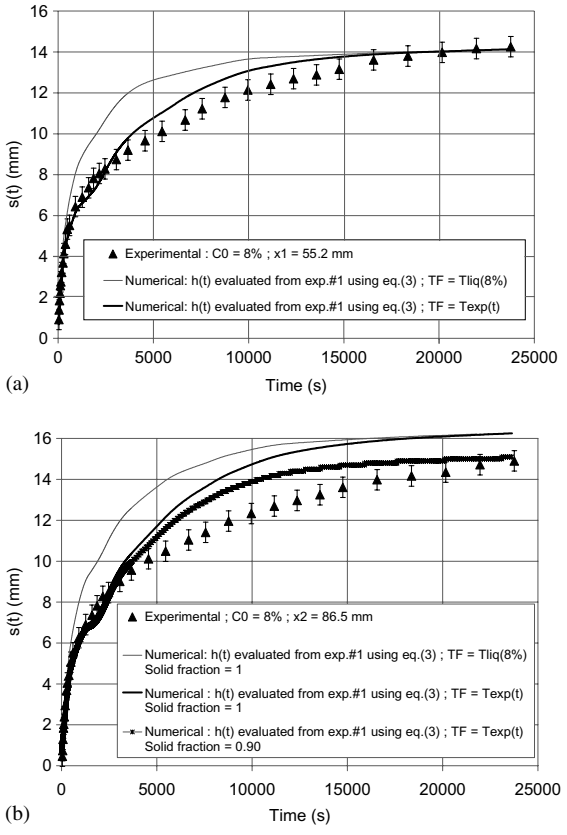

Fig. 9. Experiment #3: comparison between experimental and numerical time evolution of the front position at x_1 and x_2: (a) $x_1 = 55.2$ mm; (b) $x_2 = 86.5$ mm.

5. Conclusion

This study deals with the experimental analysis of the solidification of NH_4C_1–H_2O solution on a horizontal cold heat exchanger under a composition, temperature and velocity controlled flow (forced convection). A reference experiment (pure water) allowed for the estimation of the heat transfer coefficient at the solid/liquid interface. Experiments performed in similar thermal conditions with different concentrations (0%, 4%, 8%) showed the effect of the solute redistribution on the time evolution of the front temperature and position. The solute rejected at the solid/liquid interface leads to a significant decrease in the equilibrium temperature slowing down the solidification process. Moreover, numerical results performed with a 1D finite volume code confirmed the role of the solute redistribution on the solidification process and pointed out the effect of the solid fraction on the front kinetic. Indeed, an increase in the initial concentration leads to a decrease in the volumic solid fraction giving rise to a decrease in the solidification rate. Additional experiments are performed to emphasize those results and a more realistic modelization is developed taking into account time evolution of a non-uniform solid fraction in the solid phase.

References

[1] S.H. Davis, H.E. Huppert, U. Müller, M.G. Worster, in: Interactive Dynamics of Convection and Solidification, vol. 219, Kluwer Academic Publishers, 1992.

[2] P.J. Prescott, F.P. Incropera, Convective transport phenomena and macrosegregation during solidification of a binary metal alloy: II—Experiments and comparisons with numerical predictions, ASME J. Heat Transfer 116 (1994) 742–749.

[3] J. Tanny, Experimental study on the crystallization of a binary melt at the vertical boundary of an enclosure, Int. J. Heat Mass Transfer 38 (1995) 1141–1150.

[4] M. Epstein, F.B. Cheung, Complex freezing–melting interfaces in fluid flow, Ann. Rev. Fluid Mech. 15 (1983) 293–319.

[5] S.A. Forth, A.A. Wheeler, Hydrodynamic and morphological stability of the unidirectional solidification of a freezing

binary alloy: a simple model, J. Fluid Mech. 202 (1989) 339–366.

[6] S.A. Forth, A.A. Wheeler, Coupled convective and morphological instability in a simple model of the solidification of a binary alloy, including a shear flow, J. Fluid Mech. 236 (1992) 61–94.

[7] C.A. Chung, F. Chen, Morphological instability in a directionally solidifying binary solution with an imposed shear flow, J. Fluid Mech. 436 (2001) 85–106.

[8] C. Thangthieng, F.B. Cheung, Behavior of the two-phase mushy zone during freeze coating on a continuous moving plate, ASME J. Heat Transfer 124 (2002) 111–119.

[9] N. Ruperti Jr., D. Gobin, R.M. Cotta, Covalidation of integral transform and finite volume solutions in phase change problems, in: 7th Latin–American Heat and Mass Transfer Conference, Rio de Janeiro, November 3–6, 1998, pp. 659–664.